ATMOSPHERIC ENVIRONMENT: X 23 (2024) 100275

Contents lists available at ScienceDirect

Atmospheric Environment: X

journal homepage: www.journals.elsevier.com/atmospheric-environment-x

Comparing modelled and measured exhaust gas components from two LNG-powered ships

Mikko Heikkilä [a,*], Niina Kuittinen [b], Tiia Grönholm [a]

[a] Finnish Meteorological Institute, Erik Palménin aukio, Helsinki, 00560, Finland
[b] VTT Technical Research Centre of Finland, Kivimiehentie 3, Espoo, 02044, Finland

ARTICLE INFO

Keywords:
Shipping emissions
Liquefied natural gas
Modelling

ABSTRACT

Bottom-up modelling is used frequently to estimate emissions produced by seagoing vessels, and the accuracy of modelling is dependent on the data the model is trained with. Observational studies can be used to increase the model accuracy. Here we compared data from two measuring campaigns conducted on board ships that use Liquefied Natural Gas (LNG) as primary fuel in internal combustion engines (ICE) in a diesel-electric setup with values obtained from the Ship Traffic Emission Assessment Model (STEAM).

The power demand for propulsion calculated using Automatic Identification System (AIS) data matched observations reasonably. The root mean square error between the modelled and observed power demand was 759–914 kW (28.6–34.5%) for the measured ropax vessel and 1869–1916 kW (16.7–17.1%) for the large cruise vessel over four voyages while the ships were underway. The discrepancy is largely explained by the auxiliary power demand, which was 4 times higher on the large cruise vessel than the model prediction.

Using meteorological data to estimate the increase of resistance did not improve the goodness of fit between modelled and observed engine power demand. STEAM model's base-specific fuel consumption calculation method fits observed values reasonably when the engine load is over 50%, but ICEs used in constant speed mode have increased consumption at lower engine loads compared to variable speed ICEs.

The share of pilot fuel of total energy consumption was found to play a significant role in the emission factors for measured exhaust gas compounds. More accurate functions to model fuel consumption and emissions were derived using the observed data.

1. Introduction

"All models are wrong, but some are useful" is the famous aphorism written by statistician George Box in his 1987 book Empirical Model-Building and Response Surfaces (Box and Draper, 1987). "In any feedback loop it is, of course, the error signal – for example, the discrepancy between what tentative theory suggests should be so and what practice says is so – that can produce learning" (Box, 1976). These phrases are still topical and applied here to ship emissions. As it is impossible to go and measure the direct emissions of all ships, modelling provides valuable information on the fleet-level emissions. The results of a new measuring study can be compared to the modelled output to detect and correct the model's error.

New shipping emission models with different methods and parameters have been developed and published recently (Jalkanen et al., 2009, 2012; Johansson et al., 2017; Guo et al., 2022; Kim et al., 2023). The emission models have proven their usefulness as the shipping industry has been hesitant to release data on their environmental impact. The International Maritime Organisation (IMO) has been collecting ship fuel consumption since 2019, but only annual numbers divided by vessel and fuel type are released open-sourced. Similarly, the European Union mandates ships operating in its waters to report fuel consumption to the Monitoring, Reporting and Verifying (MRV) database. Annual numbers for each vessel are open-sourced but limited to voyages within, from or to member state ports. As most voyages are conducted on international waters, emission data is missing from national inventories. As models are as good as the underlying data that the model has been trained with, the accuracy and number of emission measurement studies define the error level in the model outcomes.

Most ships are powered by marine internal combustion engines (ICE) burning fossil fuels that produce air pollutants (particles, nitrogen oxides, sulphur, carbon monoxide and volatile organic compounds) and

* Corresponding author.
E-mail address: mikko.heikkila@fmi.fi (M. Heikkilä).

https://doi.org/10.1016/j.aeaoa.2024.100275
Received 18 March 2024; Received in revised form 21 May 2024; Accepted 24 June 2024
Available online 27 June 2024

greenhouse gases such as carbon dioxide (CO_2), methane (CH_4) and nitrous oxide (N_2O). Vessels using liquefied natural gas (LNG) as fuel release also uncombusted hydrocarbons into the atmosphere. LNG comprises mostly CH_4 that has a global warming potential (GWP) 28–36 times more than CO_2 on a 100-year horizon and 86 times more in a 20-year horizon (IPCC, 2014). CH_4 slip from marine ICEs has been studied in laboratory settings (Jensen et al., 1999; Nielsen et al., 2010; Stenersen and Thonstad, 2017), in onboard measuring studies (Anderson et al., 2015; Sommer et al., 2019; Peng et al., 2020; Balcombe et al., 2022; Lehtoranta et al., 2023; Rochussen et al., 2023; Altarriba et al., 2024), and also using remote sensing (Grönholm et al., 2021; Comer et al., 2024). The combined knowledge of the subject has been synthesized in reviews and reports (Ushakov et al., 2019; Pavlenko et al., 2020; Faber et al., 2020) and in a recent review as part of the European Union-funded GREEN RAY project (Kuittinen et al., 2023).

LNG is currently mostly used on board gas tankers carrying LNG and thus benefiting from the boil-off gas vaporising from the cargo tank, but its use on other ship types has increased (Kuittinen et al., 2023; Comer et al., 2024). The environmental benefits of combusting LNG instead of fuel oils are reductions in CO_2, sulphur dioxide (SO_2), particulate matter (PM), and nitrogen oxides (NO_x) (e.g. Burel et al., 2013; Sharafian et al., 2019; Aakko-Saksa et al., 2023; Alanen et al., 2020; Thomson et al., 2015). As CH_4 slip is not accounted for in the energy efficiency design index (EEDI), LNG offers possibilities for new vessels (Ekanem Attah and Bucknall, 2015). Besides CH_4 slip, LNG-powered dual-fuel engines have been shown to produce significantly more carbon monoxide (CO) and formaldehyde (HCOH) than fuel oil-powered ICEs (Peng et al., 2020).

Ships use ICEs in different setups - the most common having a main engine for propulsion and auxiliary engines for power production also referred to as conventional propulsion systems. Another setup is like a power station: ICEs are connected to generators that produce power for both propulsion and auxiliary needs. These are referred to as diesel-electric propulsion systems. The main difference in the ICEs for these two setups is variability in main engine speed. In the conventional setup engine revolutions can be altered with varying loads, whereas in the diesel-electric setup, engine speed is kept constant. This difference leads to differences in fuel consumption as a function of load. Also, in the diesel-electric setup, the auxiliary power demand is added to the propulsion power demand, which leads to increased load.

Many emissions have been shown to have an engine load dependency: typically relative emissions (g kWh^{-1}) increase with a decrease in load (Grigoriadis et al., 2021). Fuel oil-powered ICEs have been studied extensively, and their emissions can be modelled to a reasonable degree of accuracy using AIS-based bottom-up modelling (Moreno-Gutiérrez et al., 2015; Nunes et al., 2017; Moreno-Gutiérrez and Durán-Grados, 2021; Chen and Yang, 2024). However, a knowledge gap exists in the emission factors of LNG-powered ICEs. Ships using LNG as fuel will have to pay for their CH_4 slip for voyages into and from the European Union and within member state ports as part of the emission trading system (ETS) from 2026 onwards and as part of the directive 2023/1805 also known as the FuelEU Maritime regulation (Regulation (EU) 2023/1805, 2023). Accurate emission factors for CH_4 slip and other pollutants are needed for different vessel types and engine setups for modelling and monitoring purposes. In our understanding, this is the first study comparing directly modelled and observed emission data from LNG-powered dual-fuel engines in a diesel-electric setup. The main aim is to quantify the inaccuracy between the bottom-up model and the measured engine load, fuel consumption and emissions. Also, the more accurate functions based on the measured data were derived for the model.

2. Data and methods

Two measurement campaigns were conducted on board two ships that use LNG as primary fuel as part of the GREEN RAY project. Both vessels are diesel-electric and have 4 or 5 main engines used in operation. Exhaust gas concentrations were measured from the exhaust line of one engine at a time. A total of three different engines in two ships were monitored.

Measured components included CH_4, CO_2, CO, NO_x, and HCOH, which could be used for comparison between observed and modelled values. CH_4 concentration was measured with two different measuring devices, gas chromatography (GC, Agilent MicroGC, Santa Clara, CA, USA) and Fourier-transform infrared spectroscopy (FTIR, DX4000 by Gasmet). Horiba PG-250A analyzer was used to study NO_x (chemiluminescence detector) and CO_2 and CO (nondispersive infrared analyzer). A detailed information on instrumental set-up can be found in Lehtoranta et al. (2023).

2.1. Measuring campaign 1

The first campaign was conducted in December 2022 on board a modern LNG-powered ropax ferry that operates on a regular route between Finland and Sweden. The results of the campaign were reported by Lehtoranta et al. (2023). The vessel has four ICEs of the same type: 8-cylinder dual-fuel V-engines with a bore of 31 cm and a maximum engine power output of 4400 kW at 750 rpm. The ICEs are connected to generators with a maximum electric power output of 4224 kW. The exhaust gases were monitored from two of these engines, ME3 and ME4. The engine ME3 is a development version of this engine type with technological enhancements implemented to minimise the CH_4 slip. The engine ME4 is the standard version. In addition to the ICEs, the vessel has a power storage unit with a capacity of 2.3 MWh and the capability to connect to shore power while alongside. The vessel uses two 5.8 MW azimuthing electric-driven units for propulsion and two 1.5 MW thrusters for manoeuvring.

Measured components included CH_4, CO_2, CO, NO_x, and HCOH, which could be used for comparison between observed and modelled values. CH_4 concentration was measured with two different measuring devices, gas chromatography (GC) and Fourier-transform infrared spectroscopy (FTIR). Detailed information on instrumental set-up can be found in Lehtoranta et al. (2023).

The measuring campaign 1 aimed to produce emission factors for fixed load points. The load points for ME3 were: 10.3%, 26.0%, 51.0%, 76.0% and 88.0% and for ME4: 10.0%, 26.0%, 51.5%, 76.0% and 87.0%. Emission factors were computed using the carbon balance method described in the NO_x Technical Code of the International Maritime Organisation (2008). The method utilizes fuel chemical composition together with fuel consumption, which was available only for the fixed load points. In addition to the fixed point data, a time series of exhaust gas component concentrations from ME3 was available for one day, on which the vessel made two voyages between its regular ports of call. Engine power output and load data were available for two measuring days and four voyages. Fuel consumption for the concentration time series dataset was modelled using linear regression from the fixed load point data.

The LNG used on board had a carbon mass content of 75.3% and a hydrogen mass content of 24.6%. The pilot fuel used on board was marine diesel oil (MDO) with a carbon mass content of 84.4% and hydrogen mass content of 14.0%.

2.2. Measuring campaign 2

The second campaign was conducted in May 2023 on board a large cruise passenger vessel operating in the Mediterranean. The manuscript presenting the results was in preparation at the time this study was made. The vessel has 5 ICEs that are 14-cylinder dual-fuel V-engines with a bore of 46 cm and a maximum power output of 16030 kW at 600 rpm. The ICEs are connected to generators with a maximum electric power output of 14427 kW each. The ship uses two 25 MW propulsion electric motors (PEM) and is fitted with 7 thrusters for manoeuvring. The vessel is capable of using shore power but did not use it during the measuring campaign. This enabled a comparison of modelled and measured auxiliary power on board.

Exhaust gas measurements were conducted on a single ICE (DG5) during the whole campaign, and the instruments used were the same as in the first campaign. DG5 is a standard constant speed off-the-shelf 4-stroke low-pressure dual-fuel ICE.

As with the first measuring campaign, the second campaign also produced emission factors for fixed load points. These points for DG5 were: 9.6%, 24.3%, 52.9%, 53.6%, 72.7%, 78.8% and 79.2%. As per company policy, the engines were not used above 82.0% generator load. Measuring was done using LNG and low-sulphur Marine Gas Oil (MGO) to compare the difference in exhaust gas compound outputs between the two fuels. Time series of exhaust gas concentration data was available for the whole campaign together with fuel consumption data with a 5-min resolution.

The LNG used on board had a mass carbon content of 75.1% and a mass hydrogen content of 24.8%. The pilot fuel used on board was marine gas oil (MGO) with a mass carbon content of 86.7% and hydrogen mass content of 13.5%.

2.3. STEAM model

The Shipping Traffic Emissions Assessment Model (STEAM) was first introduced in 2009 to assess the air emissions produced by maritime transport in the Baltic Sea area by combining Automatic Identification System (AIS) data with a ship database and emission factors (Jalkanen et al., 2009). The model has been updated using more precise knowledge of different vessel types, and more pollutants and also extending the coverage to the global maritime fleet (Jalkanen et al., 2012; Johansson et al., 2017).

The emissions from both vessels were modelled with STEAM using Automatic Identification System (AIS) data purchased from Orbcomm and VesselFinder, vessel specifications purchased from IHS Markit, and historical meteorological data obtained from Copernicus Marine Services.

STEAM is a bottom-up method model, which calculates the ship's resistance through water using methods described by Hollenbach (1999). The added resistance caused by meteorological parameters, such as wind, waves and currents, are calculated using methods developed by Blendermann (1994) and Townsin and Kwon (1983, 1993) as described by Jalkanen et al. (2009) and of ice by methods developed by Riska et al. (1997); Juva and Riska (2002). Using modelled resistance STEAM calculates the power demand for the propulsion. For a diesel-electric vessel such as the two measured ships in campaigns 1 and 2, the auxiliary power demand is added to the propulsion power demand. In a multi-engine setup, STEAM divides the power demand between engines and uses 85% of engine load as cut-off, where a new engine is brought online. A minimum of 2 engines are modelled to be online when the ship is underway. STEAM calculates the fuel consumption of LNG-powered ships by multiplying the Base Specific Energy Consumption ($BSEC_{Base}$) in kilojoules per kilowatt-hour with the unitless Relative Base Specific Energy Consumption ($BSEC_{Relative}$):

$$\mathrm{BSEC}\left(\frac{kJ}{kWh}\right) = BSEC_{Base}\left(\frac{kJ}{kWh}\right)\cdot BSEC_{Relative}, \tag{1}$$

where $BSEC_{Relative}$ is:

$$\mathrm{BSEC}_{Relative} = \alpha\cdot L^2 + \beta\cdot L + \gamma, \tag{2}$$

where L is the engine load (actual power/maximum power), $\alpha = 0.45$, $\beta = -0.71$, and $\gamma = 1.28$.

$BSEC_{Base}$ values for each engine type are collected from the engine manufacturers' websites and product catalogues. The same $BSEC_{Relative}$ for constant and variable speed ICEs is used in STEAM. Moreover, all fuel consumed by LNG-powered ships with dual-fuel engines is assumed to be LNG and the share of pilot fuel consumed is not taken into account in STEAM. Also, based on the observations of Anderson et al. (2015), STEAM assumes LNG-powered dual-fuel engines switch fuel to MGO, when the engine load is $< 20\%$, and emissions that occur below this point are modelled with MGO-based emission factors.

STEAM uses emission factors reported by Grigoriadis et al. (2021) to model different exhaust gas components with a few exceptions for LNG-powered ships. For CH_4 slip, STEAM categorises ICEs by their built year into two groups: engines manufactured before and after 2010. Further, different factors are used for the four different dual-fuel piston engine types: lean-burn spark plug ignited engines (group 1), low-pressure otto cycle 4-stroke engines (group 2), low-pressure otto cycle 2-stroke engines (group 3) and high-pressure diesel cycle 2-stroke engines (group 4). As the ICEs used on board the measured vessels belong to group 2 and were built after 2010, STEAM models their CH_4 emission as a constant 3.7% slip of consumed fuel based on the works of Nielsen and Stenersen (2010) and Stenersen and Thonstad (2017). This leads to a linear CH_4 emission as a function of engine load. As STEAM assumes the engine does not consume LNG gas at low engine loads $< 20\%$, it obviously estimates zero CH_4 emissions for this load range.

CO_2 emission factor (in g kWh^{-1}) in STEAM is modelled as:

$$EF_{CO_2} = FCC\cdot SFOC\cdot\frac{M_{CO_2}}{M_C}, \tag{3}$$

where FCC is the fuel carbon content (0.75 for LNG), SFOC is the specific fuel oil consumption (in g kWh^{-1}), M_{CO_2} is the molar mass of CO_2 (44.01 g mol^{-1}) and M_C is the molar mass of carbon (12.01 g mol^{-1}). SFOC is derived from BSEC using the lower heating value (LHV) for LNG (49.79 kJ g^{-1}).

CO emission factor for CO (EF_{CO} in g kWh^{-1}) is modelled in STEAM as a function of engine load:

$$EF_{CO} = EF_{Base}(\alpha\cdot L^2 + \beta\cdot L + \gamma), \tag{4}$$

where L is the engine load (actual power/maximum power), $EF_{Base} = 3.800$, $\alpha = 2.559$, $\beta = -4.623$ and $\gamma = 2.440$.

NO_x emissions for medium-speed ICEs (130–2000 rpm) are modelled in STEAM as a function of engine load. If the load is $> 50\%$:

$$EF_{NO_x} = EF_{Base} \tag{5}$$

and when the load is $\leq 50\%$:

$$EF_{NO_x} = EF_{Base}(\alpha\cdot L^2 + \beta\cdot L + \gamma), \tag{6}$$

where EF_{NO_x} is the emission factor for NO_x (g kWh^{-1}), L is the engine load (actual power/maximum power), $\alpha = 4.14$, $\beta = -4.14$, $\gamma = 2.03$, and EF_{Base} is modelled as a function of engine maximum speed when the ship is in Nitrogen Oxides Emission Control Area (NECA):

$$EF_{Base} = 47.2\cdot \mathrm{rpm}^{-0.244}, \tag{7}$$

and when the ship is not in NECA:

$$EF_{Base} = 35.1\cdot \mathrm{rpm}^{-0.234}, \tag{8}$$

where EF_{Base} is the base emission factor and rpm is the engine's maximum speed. Formulas 7 and 8 yield $EF_{Base} = 9.385$ for the vessel in campaign 1 and $EF_{Base} = 7.856$ for the vessel in campaign 2. NO_x emissions of LNG-powered ships are modelled with reduction factors: for group 1, 2, 3, and 4 engines the reduction factor is 90%, 85%, 85%, and 30%, respectively.

STEAM models non-methane volatile organic compounds (NMVOC) in groups without a separate emission factor for HCOH.

Two datasets by STEAM-model were created for both campaigns: one without the impact of meteorological parameters and the other with the weather impact included.

2.4. Comparing measured and modelled values

Engine power output in normal operation at sea during the measuring campaigns was compared with the results of STEAM-runs to define the accuracy of resistance modelling through the water and the impact of resistance caused by meteorological parameters. Engine power outputs of modelled and observed values while the vessels were in port were compared to define the accuracy of STEAM's method to estimate the auxiliary power demand. The time resolution of observed values varied between the two vessels and with the resolution of the measuring instruments. In contrast, the time resolution of modelled values varied with the resolution of the underlying AIS data. As these resolutions were not the same, the modelled STEAM values were interpolated to the time resolution of observed data. Modelled and observed values were compared using Pearson's correlation, root mean square error and adjusted r^2 of linear regression.

Observed and modelled energy consumption were compared by calculating the $BSEC_{Relative}$ of the measured engine and comparing it to Formula 2 used by STEAM. Energy consumption from the first measuring campaign was available for the fixed load points and two different engines, whereas for the second campaign, it was available for the whole campaign providing more data points for comparison. In addition, the ratio of pilot fuel consumption to the total energy consumed ($E_{pilot}\ E_{total}{}^{-1}$) was compared between the measured and modelled values for all three measured engines.

Measured concentrations of each exhaust gas compound were converted to emission rates (g s^{-1}) using the NO_x Technical Code (International Maritime Organisation, 2008) carbon balance method (IMO method, EF_{IMO}). The NO_x Technical Code uses density ratios (coefficient u_{gas}) of exhaust gas compounds and the combusted fuel and these ratios are provided in Table 5 for CO_2, CO, O_2, NO_x and other hydrocarbons (HC). Density ratios were calculated for CH_4 and HCOH and presented in Table 1.

The actual combusted LNG gas was calculated by subtracting the CH_4 slip from the gas consumption. CO_2 and NO_x emission rates (g s^{-1}) were calculated as a combination of combusted LNG gas and pilot fuel. As the carbon content of the LNG and pilot fuel varies, a correction factor for CO_2 emissions was calculated as a function of engine load using linear regression. Energy-based emission factors for CO and HCOH emissions were calculated (g kWh^{-1}) as a function of engine load to produce more accurate emission factor formulas for modelling.

Besides the IMO method, we used the ratio of compound and CO_2 to express the emission. We call this method for calculating the emission factor the molar mass method (EF_{mm}) and compare the results to those by the IMO method. As the ambient pressure and temperature of measured gases are the same, the conversion can be done using the ideal gas law:

$$EF_X = \frac{\Delta X(ppm)}{\Delta CO_2(ppm)} \cdot F_f, \tag{9}$$

where EF_X is the emission factor for compound X (g X g $fuel^{-1}$), ΔX (ppm) is the measured concentration of compound X, ΔCO_2 (ppm) is the measured concentration of carbon dioxide, and F_f is the fuel factor that can be calculated as:

$$F_f = \frac{M_X}{M_{CO_2}} \cdot C_f, \tag{10}$$

where M_X is the molar mass of compound X, M_{CO_2} is the molar mass of carbon dioxide and C_f is the carbon dioxide emission factor of LNG (g CO_2 g $fuel^{-1}$). Molar mass of CO_2 is 44.01 g mol^{-1}, CH_4 is 16.04 g mol^{-1}, CO is 28.01 g mol^{-1} and of HCOH is 30.03 g mol^{-1}. C_f is calculated as:

$$C_f = \frac{M_{CO_2}}{M_C} \cdot FCC, \tag{11}$$

where M_{CO_2} is the molar mass of CO_2, M_C is the molar mass of carbon (12.01 g mol^{-1}) and FCC is fuel carbon content (g C g $fuel^{-1}$). As per the IMO, the default FCC of LNG is 0.75 and of MGO 0.87 (International Maritime Organisation, 2008). Therefore the calculated C_f of LNG is 2.75 and of MGO 3.19. Table 2 presents calculated F_f for different exhaust gas compounds and typical marine fuels.

Ship operational status was identified by the speed of the vessel: if speed was < 0.2 knots, the vessel was labelled as berthed alongside in port, if $0.2 \leq$ speed < 6.0 knots, the vessel was labelled as manoeuvring and if speed ≥ 6.0 knots, the vessel was labelled as sailing. Concentrations of exhaust gas components were investigated between these groups to identify potential sources for outlier concentrations.

3. Results

For campaign 1, STEAM model overpredicts emissions of all compared exhaust gas compounds (CO_2, CO, CH_4 and NO_x) and also energy consumed in kilowatt-hours and fuel consumed in megajoules (Table 3 and Fig. 1). The comparison includes one day with two voyages between ports for the development engine ME3. For campaign 2, STEAM model overpredicts emissions of CO_2, CO and CH_4 and underpredicts emissions of NO_x, energy consumed in kilowatt-hours and fuel consumed in megajoules (Table 3 and Fig. 2). The comparison includes four days and four voyages between ports for the engine DG5. Each of these comparisons is looked at in more detail in the following sections.

Table 2
Calculated fuel factors (F_f) for different exhaust gas compounds and typical marine fuels (HFO: Heavy Fuel Oil, LFO: Light Fuel Oil, MGO: Marine Gas oil, LNG: Liquefied Natural Gas) used on ships. Calculations were conducted using default fuel carbon content values (FCC).

Gas	F_f HFO	F_f LFO	F_f MGO	F_f LNG
FCC	0.85	0.86	0.87	0.75
CH_4	1.14	1.15	1.16	1.00
CO	1.98	2.01	2.03	1.75
HCOH	2.34	2.37	2.17	1.87
NO	2.12	2.15	2.17	1.87
NO_2	3.26	3.29	3.33	2.87
SO_2	4.53	4.59	4.64	4.00

The greatest advantage of the method is that concentrations of different compounds can be converted to fuel-based emission factors without the need for fuel consumption data.

Table 1
Coefficient u_{gas} for liquid fuels (LF) and natural gas (NG) and for nitrogen oxides (NO_x), carbon monoxide (CO), hydrocarbons (HC) and carbon dioxide (CO_2) as provided in Table 5 of the IMO NO_x Technical Code and calculated for formaldehyde (HCOH) and methane (CH_4).

Fuel	NO_x	CO	HC	CO_2	HCOH	CH_4
LF	0.001586	0.000966	0.000479	0.001517	0.001035	0.000552
NG	0.001621	0.000987	0.000558	0.001551	0.001058	0.000564

CH_4 slip (g g $fuel^{-1}$) was calculated by dividing the CH_4 output (g s^{-1}) with the gas consumption. A regression curve for measured CH_4 slip and engine load was fitted to obtain a formula for modelling.

Table 3
Differences in per cent between cumulative modelled and observed values from campaigns 1 and 2 for STEAM model without weather impact (STEAM) and with weather impact (STEAM W).

Campaign	Model	CO_2	CO	CH_4	NO_x	kWh	MJ
1	STEAM	163%	579%	1001%	2212%	50%	26%
1	STEAM W	172%	585%	1041%	2296%	53%	29%
2	STEAM	29%	150%	281%	−29%	−28%	−10%
2	STEAM W	38%	174%	310%	−26%	−28%	−10%

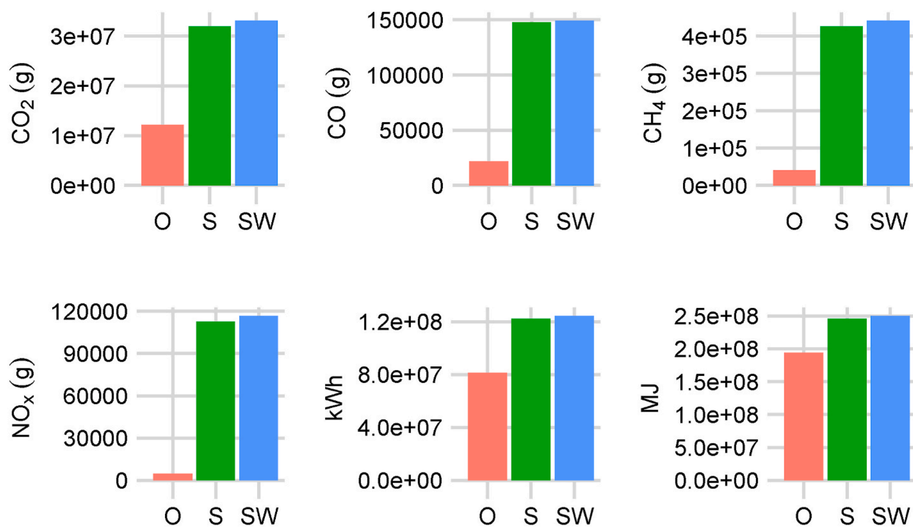

Fig. 1. Cumulative observed (O) and modelled (S: STEAM, SW: STEAM with weather) emissions of CO_2 (top left), CO (top centre), CH_4 (top right) and NO_x (bottom left), cumulative consumed energy in kilowatt-hours (bottom centre) and consumed fuel in megajoules (bottom right) of the vessel measured during campaign 1.

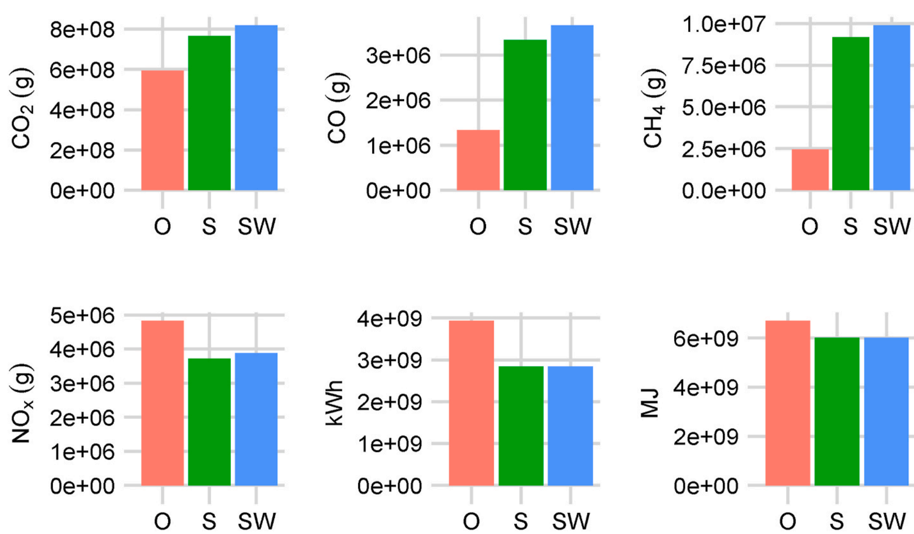

Fig. 2. Cumulative observed (O) and modelled (S: STEAM, SW: STEAM with weather) emissions of CO_2 (top left), CO (top centre), CH_4 (top right) and NO_x (bottom left), cumulative energy in kilowatt-hours (bottom centre) and consumed fuel in megajoules (bottom right) of the vessel measured during campaign 2.

3.1. Engine load

STEAM model is sensitive to all changes in speed, which creates additional noise in the data compared to the actual power demand. The noise can be observed in comparisons of both measuring campaigns and decreases the adjusted r^2 between modelled and observed values (0.13 − 0.57) while the ships were moving. However, the overall goodness of fit is reasonable: the correlation ranges from 0.36 to 0.75 (95% confidence interval 0.31 − 0.77) and the root mean square error (RMSE) was 759 − 914 kW for campaign 1 and 1869–1916 kW for campaign 2. Adjusting the resistance experienced by the vessel by weather did not improve the model accuracy (Table 4).

The ropax ferry that was measured in campaign 1 connects to shore power while alongside in port and the power demand of the ICEs decreases to zero. STEAM assumes this to happen only if the stay in port is longer than 8 h. Therefore, the modelled engine power demand matches the observed power during the overnight stay in port, but not during the shorter port call between two voyages. The voyage consists of speed-restricted parts leading to high variability in the engine load. During the first voyage, STEAM seems to underpredict power demand most of

Table 4
Pearson's correlation (R) with 95% confidence intervals, root mean square error (RMSE), root mean square error in percentage (RMSE %) and r^2 of linear regression between observed and STEAM modelled main engine power (kW) for campaigns 1 and 2 without weather impact (STEAM) and with weather (STEAM W) while the ships were moving.

Campaign	Model	R	95%CI		RMSE	RMSE %	R^2
1	STEAM	0.47	0.41	0.52	759	28.6	0.22
1	STEAM W	0.36	0.31	0.42	914	34.5	0.13
2	STEAM	0.70	0.69	0.71	1869	16.7	0.57
2	STEAM W	0.73	0.70	0.76	1916	17.1	0.53

the time and overpredict during the manoeuvring phase. During the second voyage, STEAM seemed to overpredict the whole voyage especially when meteorological impact was used. The wind was gusting over 20 m per second during the second voyage. Underprediction during the first voyage could be explained by uncertainty in modelling the resistance through the water or by underestimating the auxiliary power demand. However, the overprediction during the second voyage contradicts this explanation. Overprediction could also be caused by the vessel using the power storage system (Fig. 3).

As with the first measuring campaign, the modelled engine load during the second campaign varies heavily with changes in speed whereas the observed load is more constant. Meteorological impact smoothens out some of the noise. As the measured vessel does not connect to shore power during port calls, the auxiliary power demand can be observed from the observed power demand. The STEAM model underestimates the auxiliary power demand by a factor of 4: the observed power demand while alongside in port was 8300–9000 kW whereas STEAM models only 2350 kW. This leads to an underprediction also while the ship is at sea, although it is divided between all the engines that are modelled to be online. The modelled power demand seems to match the observed during the manoeuvring phase of the voyage, but this is an artefact of the ship having more engines online than what STEAM predicts (Fig. 4).

3.2. Fuel consumption

Fuel consumption of an LNG-powered dual-fuel engine consists of the LNG gas consumption together with the pilot fuel consumption. As STEAM does not model the pilot fuel and assumes all fuel consumed to be LNG, observed gas and pilot fuel were first calculated as total energy

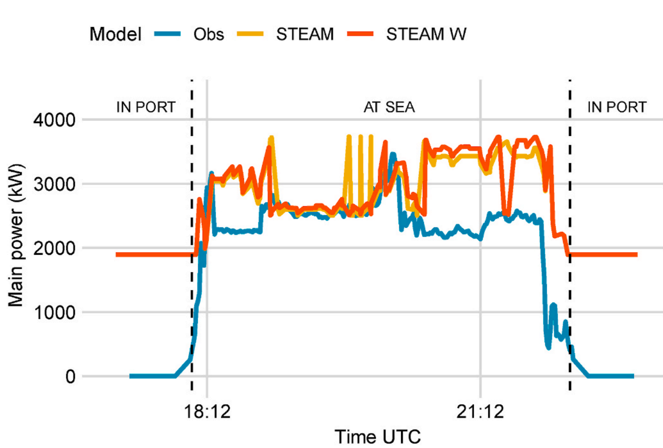

Fig. 3. Modelled and observed main engine power demand (kW) from the first measuring campaign on board a diesel-electric ropax ferry during one voyage. Observed power demand with green line, STEAM modelled power demand without weather impact (STEAM) with yellow line and STEAM modelled load with weather impact (STEAM W) with red line. (For interpretation of the references to colour in this figure legend, the reader is referred to the Web version of this article.)

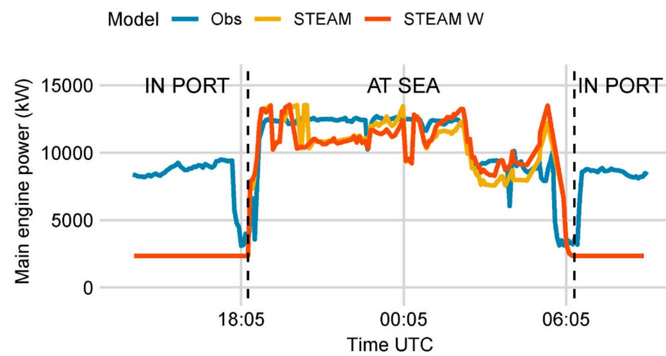

Fig. 4. Modelled and observed main engine power demand (kW) from the second measuring campaign on board a diesel-electric cruise passenger vessel during a day with both stay in port and sailing. Observed power demand with green line, STEAM modelled power demand without weather impact (STEAM) with yellow line and STEAM modelled load with weather impact (STEAM W) with red line. (For interpretation of the references to colour in this figure legend, the reader is referred to the Web version of this article.)

consumption (in MJ) with lower heating values (LHV) of 49.79 MJ kg^{-1} of fuel for LNG and 42.70 MJ kg^{-1} of fuel for MGO. For campaign 2, where fuel consumption data was available for the whole campaign, Pearson's correlation between modelled and observed total energy consumption was 0.99 (95% confidence interval 0.99 – 0.99, $p< 0.01$) with around 6% underprediction.

3.2.1. Relative energy consumption

The $BSEC_{Relative}$ (Formula 2) used by STEAM is reasonably accurate for engine loads > 50%, but with lower loads, it leads to significant underprediction of fuel consumption when observed and modelled values were compared with results from the measuring campaigns. Also, the shape of the curve does not seem parabolic, thus making a polynomial function inaccurate (Fig. 5). A partial linear exponential decay regression algorithm introduced by Golub and Pereyra (2003) was applied instead:

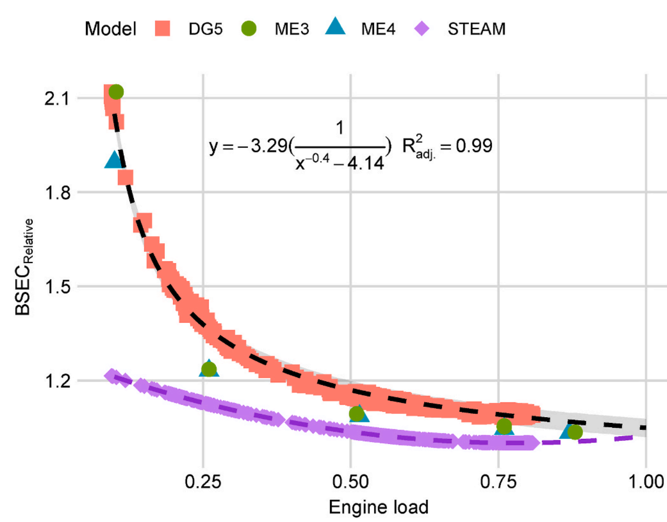

Fig. 5. Relative Base Specific Energy Consumption ($BSEC_{Relative}$) as a function of engine load of three engines (ME3, ME4 and DG5) with corresponding colours and shapes. Purple diamonds represent the STEAM modelled $BSEC_{Relative}$ values for DG5 and the purple dashed line STEAM modelled values throughout the load range using Formula 2. The black dashed line is the fitted exponential decay regression and the grey area is the 95% prediction interval for the regression. (For interpretation of the references to colour in this figure legend, the reader is referred to the Web version of this article.)

$$BSEC_{Relative} = \alpha\left(\frac{1}{L^{\beta}+\gamma}\right), \quad (12)$$

where L is the engine load (actual power/maximum power), $\alpha = -3.29$ (95% CI $-3.45 - -3.14$, p<0.01), $\beta = -0.40$ (95% CI $-0.42 - -0.39$, p<0.01) and $\gamma = -4.14$ (95% CI $-4.29 - -3.99$, p<0.01). The adjusted r^2 of the regression is 0.99, and RMSE is 0.01. The function is valid with engine loads 5%–100% and with current STEAM $BSEC_{Base}$ values (Fig. 5).

3.2.2. Share of pilot fuel

The share of pilot fuel of the total energy consumed ($E_{pilot}\ E_{total}^{-1}$) varies significantly between the three measured engines (Fig. 6) ranging from 0.7% at 80.8% engine load (DG5) to 23.2% at 10.3% engine load (ME3). $E_{pilot}\ E_{total}^{-1}$ can be modelled with a 2nd degree polynomial fit. Four models were created: one for each engine and a combination of ME4 and DG5, representing standard off-the-shelf constant-speed dual-fuel engines. The regression results are presented in Fig. 6 and in Table 5.

3.3. Methane slip

The development engine (ME3) has a reduced CH_4 slip (g CH_4 g fuel^{-1}) compared to the standard engine on board the same vessel (ME4) or the larger engine DG5 on board the ship in campaign 2. The mean CH_4 slip of ME3 during one measuring day of normal operation was 1.08 ± 0.27%, the median was 1.00% and measured CH_4 slip ranged from $3.87 \cdot 10^{-5}$ to $3.23 \cdot 10^{-2}$ (0.00% – 3.23%). The ME4 engine data was only available at fixed load points, on which the CH_4 slip ranged from 2.12% to 5.01% at 87% and 10% engine load, respectively. The mean CH_4 slip measured from the DG5 during measuring campaign 2 was 2.06 ± 1.33%, the median was 1.64% and ranging from 0.49% at 79.1% engine load to 24.06% at 15.8% engine load.

CH_4 slip (as g CH_4 g fuel^{-1}) has a clear engine load dependency but also depends on the pilot fuel share to the total energy consumption. Knowing these, the CH_4 slip can be modelled with a multivariable linear regression:

$$EF_{CH_4} = \alpha \cdot L + \beta \cdot P + \gamma, \quad (13)$$

where EF_{CH_4} is the CH_4 slip (g CH_4 g fuel^{-1}), L is the engine load (actual power/maximum power), P is the share of pilot fuel of total energy consumption, α and β are the coefficients and γ is the intercept. The predicted values of the regressions have adjusted r^2 of 0.72 (ME3), 0.94 (ME4), 0.80 (DG5) and 0.81 (all engines), but a combined regression using data for all three engines has adjusted $r^2 = 0.47$ (Table 6 and Fig. 7).

An univariable function with only engine load as the dependent variable is in many cases more useable than a multivariable with load combined with the share of pilot fuel. However, the shapes of the curves were different between the measured engines. The optimum fit for CH_4 slip from DG5 was achieved with exponential regression:

$$EF_{CH_4} = \alpha \cdot e^{\beta \cdot L} + \gamma, \quad (14)$$

while the CH_4 slip on ME3 and ME4 have a parabolic shape and the slip was modelled using polynomial regression:

$$EF_{CH_4} = \alpha \cdot L^2 + \beta \cdot L + \gamma. \quad (15)$$

In the equations above EF_{CH_4} is CH_4 slip, L is the engine load (actual power/maximum power), α and β are coefficients and γ is the intercept. The values for coefficient are Table 7 and Fig. 8 shows the data and regression curves.

3.4. Carbon dioxide

The mean emission factor for CO_2 (g g fuel^{-1}) measured from engine ME3 was 3.00 ± 0.01 with a median of 2.99 and ranging from 2.94 to 3.17. The mean emission factor for CO_2 (g g fuel^{-1}) measured from engine DG5 during campaign 2 was 2.96 ± 0.01 with a median of 2.96 and ranging from 2.76 to 2.98. As CO_2 is the product of combusting a combination of LNG gas and pilot fuel, the emission rate for CO_2 (in g s^{-1}) can be expressed as:

$$ER_{CO_2} = F_{pilot} \cdot Cf_{pilot} + F_{gas} \cdot Cf_{gas}, \quad (16)$$

where ER_{CO_2} is the emission rate of CO_2 (g s^{-1}), F_{pilot} is the consumption rate (g s^{-1}) of combusted pilot fuel, Cf_{pilot} is the emission factor of CO_2 for the pilot fuel, F_{gas} is the consumption rate (g s^{-1}) of combusted LNG gas and CF_{gas} is the CO_2 emission factor for LNG. The consumption of combusted LNG gas can be expressed as:

$$F_{combusted} = F_{consumed} \cdot (1 - CH_4 \text{ slip}) \quad (17)$$

Using the Formula 11 together with a fuel carbon content of 0.75 for LNG and 0.87 for MGO, the measured and calculated CO_2 emission have a perfect correlation (1.00, p< 0.01), but the calculated model under-predicts CO_2 emission by around 8%. Using linear regression, the emission rate for CO_2 can be expressed as:

$$ER_{CO_2} = \alpha \cdot (F_{pilot} \cdot Cf_{pilot} + F_{gas} \cdot Cf_{gas}) + \gamma, \quad (18)$$

where $\alpha = 1.08$ (95% CI 1.08 – 1.08, $p < 0.01$), $\gamma = -10.11$ (95% CI $-10.25 - -9.97$, $p < 0.01$), $Cf_{pilot} = 3.19$ and $Cf_{gas} = 2.75$.

3.5. Carbon monoxide and formaldehyde

Higher concentrations of CO and HCOH in the exhaust gas seem to occur at lower engine loads similar to the CH_4 slip. The correlation between CH_4 (ppm) and CO (ppm) during campaign 1 was 0.52 (95% confidence interval 0.48 – 0.56, $p < 0.01$) and during campaign 2 0.95 (95% CI 0.95 – 0.96, $p < 0.01$). The correlation between CH_4 and HCOH during campaign 1 was 0.84 (95% CI 0.83 – 0.86, $p < 0.01$) and during campaign 2 0.97 (95% CI 0.97 – 0.97, $p < 0.01$).

The mean emission factor for CO (g kWh^{-1}) measured on engine ME3

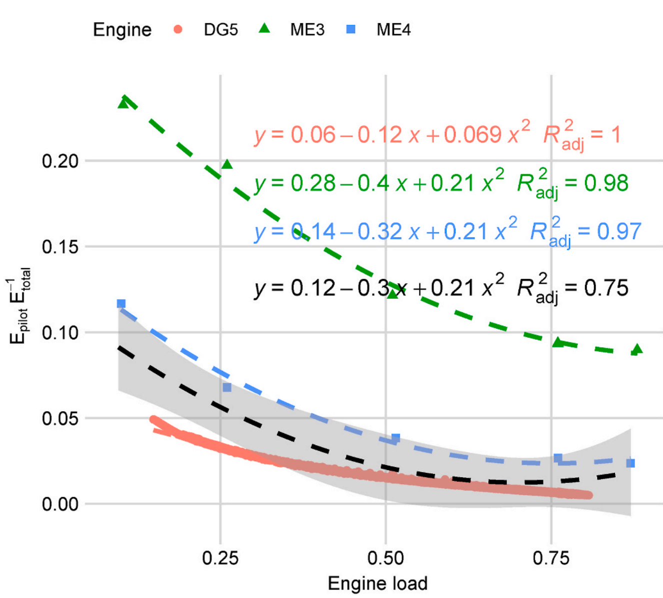

Fig. 6. Share of pilot fuel of total energy consumption ($E_{pilot}\ E_{total}^{-1}$) of the three measured engines (DG5, ME3 and ME4) as a function of engine load with corresponding colours, shapes and polynomial regressions. The black dashed line represents the combined ME4+DG5 regression calculated from the fixed load point values with the 95% confidence interval (grey area). (For interpretation of the references to colour in this figure legend, the reader is referred to the Web version of this article.)

Table 5
Measured engine, regression model coefficients α, β and γ with their 95% confidence intervals and the adjusted r^2 of the regression to predict the share of pilot fuel of the total energy consumption ($E_{pilot}\ E_{total}^{-1}$). *The regression for ME3, ME4 and the combination ME4+DG5 (Com) were calculated using only the fuel consumption values for the fixed engine load points.

Eng.	α	95%CI		β	95%CI		γ	95%CI		r^2
ME3*	0.21	0.02	0.40	−0.40	−0.59	−0.21	0.28	0.24	0.31	0.99
ME4*	0.21	−0.01	0.43	−0.32	−0.54	−0.10	0.14	0.10	0.19	0.97
DG5	0.07	0.07	0.07	−0.12	−0.12	−0.12	0.06	0.06	0.06	1.00
Com*	0.21	0.00	0.42	−0.30	−0.50	−0.10	0.12	0.08	0.16	0.75

Table 6
Coefficients (α and β) and the intercept (γ) with 95% confidence intervals for multivariable linear regression to model the CH_4 slip using engine load and share of pilot fuel as variables for 3 measured engines and a combination of all three. *Data for ME4 was available only for the fixed load points.

Eng.	α	95%CI		β	95%CI		γ	95%CI		r^2
ME3	0.02	0.02	0.02	0.11	0.12	0.13	−0.02	−0.02	−0.01	0.73
ME4*	0.00	−0.06	0.06	0.33	−0.16	0.81	0.01	−0.04	0.07	0.94
DG5	0.10	0.10	0.10	3.30	3.25	3.35	−0.08	−0.08	−0.08	0.80
All	−0.05	−0.06	−0.05	−0.10	−0.11	−0.10	0.06	0.06	0.06	0.47

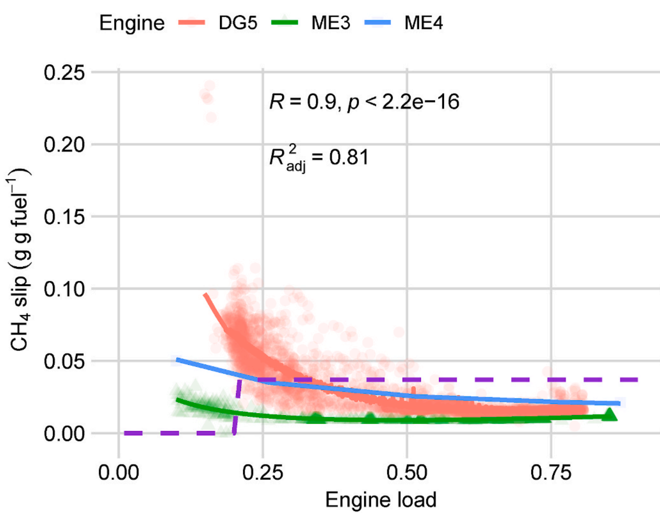

Fig. 7. CH_4 slip (g g fuel^{-1}) measured from engines DG5 (orange points), ME3 (green triangles) and ME4 (blue squares) and fitted multivariable linear regression using engine load and share of pilot fuel as variables (solid lines with corresponding colours). The current STEAM CH_4 slip is marked with a purple dashed line. (For interpretation of the references to colour in this figure legend, the reader is referred to the Web version of this article.)

was 1.32 ± 1.75, the median 0.75 and ranging from 0.52 to 12.03. The mean emission factor of HCOH (mg kWh^{-1}) measured on engine ME3 was 103.23 ± 66.70, with a median of 84.20 ranging from 11.05 to 625.22. The mean emission factor for CO (g kWh^{-1}) measured on engine DG5 while the engine was running on LNG was 1.67 ± 0.82, the median 1.41 and ranging from 0.90 to 16.37. The mean emission factor of HCOH (mg kWh^{-1}) measured on engine DG5 during campaign 2 was 214.19 ± 94.08, with a median of 187.02 and ranging from 87.53 to 1840.50.

The emission factor for CO (g kWh^{-1}) can be modelled as:

$$EF_{CO} = EF_{Base} \cdot EF_{Relative}, \tag{19}$$

where EF_{Base} is defined as the median of measured CO (g kWh^{-1}). These were 0.75 for ME3 and 1.41 for DG5. $EF_{Relative}$ can be modelled as:

$$EF_{Relative} = \alpha \cdot L^{\beta}, \tag{20}$$

where L is the engine load (actual power/maximum power), $\alpha = 0.53$ (95% CI 0.52 − 0.54, $p < 0.01$) and $\beta = -1.28$ (95% CI −1.30 − −1.27, $p < 0.01$). The adjusted r^2 for all three engines is 0.53 and RMSE 1.95.

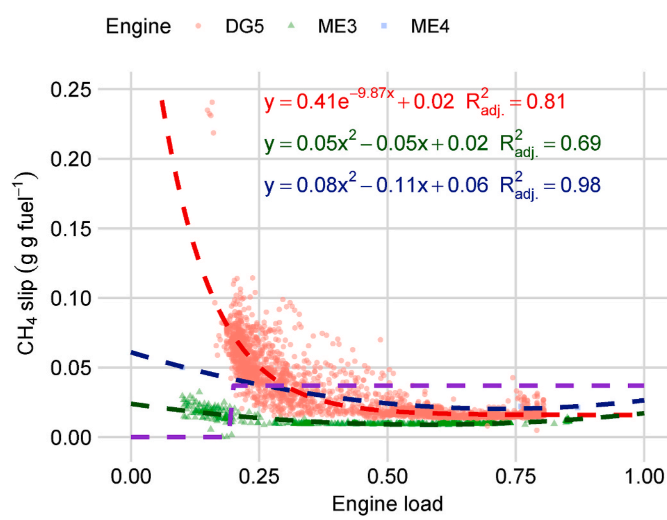

Fig. 8. CH_4 slip (g g fuel^{-1}) calculated from the measurements of DG5 (orange circles), ME3 (green triangles) and ME4 (blue squares) with fitted polynomial regressions in corresponding colours (dashed lines). The purple dashed line represents STEAM-modelled methane slip for 4-stroke low-pressure LNG-powered engines. (For interpretation of the references to colour in this figure legend, the reader is referred to the Web version of this article.)

Table 7
Measured engine, regression model coefficients α, β and γ with their 95% confidence intervals and the adjusted r^2 of the regression to predict the CH_4 slip of three different types of LNG-powered dual fuel internal combustion engines. *The regression for ME4 was calculated using only the CH_4 slip values for the fixed engine load points.

Eng.	α	95%CI		β	95%CI		γ	95%CI		r^2
ME3	0.05	0.04	0.05	−0.05	−0.05	−0.05	0.02	0.02	0.02	0.69
ME4*	0.08	0.02	0.14	−0.11	−0.17	−0.05	0.06	0.05	0.07	0.98
DG5	0.41	0.39	0.43	−9.87	−9.62	−10.13	0.02	0.02	0.02	0.81

For ME3 adjusted r^2 is 0.74 and RMSE 1.52, for ME4 adjusted r^2 is 1.00 and RMSE 6.74 and for DG5 adjusted r^2 is 0.77 and RMSE 1.96 (Fig. 9).

The emission factor for HCOH (mg kWh^{-1}) can be modelled as:

$$EF_{HCOH} = EF_{Base} \cdot EF_{Relative}, \tag{21}$$

where EF_{Base} is defined as the median of measured HCOH (mg kWh^{-1}). These were 84.20 for ME3, 106.73 for ME4 and 187.02 for DG5. $EF_{Relative}$ can be modelled as:

$$EF_{Relative} = \alpha \cdot L^{\beta}, \tag{22}$$

where L is the engine load (actual power divided by maximum power), $\alpha = 0.69$ (95% CI 0.68 – 0.69, $p < 0.01$) and $\beta = -0.86$ (95% CI – 0.86 – –0.85, $p < 0.01$). The adjusted r^2 for all engines is 0.79 and RMSE is 45.12. For ME3 adjusted r^2 is 0.66 and RMSE 39.90, for ME4 adjusted r^2 is 0.99 and RMSE 19.92, and for DG5 adjusted r^2 is 0.76 and RMSE 45.74 (Fig. 10).

3.6. Nitrogen oxides

The NO_x emission factors (in g kWh^{-1}) followed very different curves between the three measured engines and no general conclusions could be drawn. The mean emission rate of NO_x measured from engine ME3 during campaign 1 was 0.15 ± 0.14 (g s^{-1}) with a median of 0.16 and ranging from 0.02 to 2.75. The distribution of the measurements was highly skewed as at times when the engine was started and stopped, significantly higher emission rates occurred. These episodes were omitted from the emission rate modelling and the data was normalised by subsetting the values to <1 g s^{-1}. The NO_x emission rates were available only at fixed engine load points for the engine ME4. The mean emission rate for NO_x measured from engine DG5 during campaign 2 was 5.91 ± 1.68 (g s^{-1}) with a median of 5.47 and ranging from 0.06 to 15.43. The distribution of measured values was closer to normal as the engine was not turned off during the campaign. As the nitrogen oxides are a product of combusting a mixture of gas and pilot fuel, the emission rate can be modelled as:

$$ER_{NO_x} = \alpha \cdot F_{gas} + \beta \cdot F_{pilot} + \gamma, \tag{23}$$

where ER_{NO_x} is the emission rate (in g s^{-1}), F_{gas} is the gas fuel combustion rate (in g s^{-1} taking in account the CH_4 slip using formula 17), F_{pilot} is the pilot fuel consumption rate (in g s^{-1}), α and β are the coefficients and γ is the intercept. The obtained coefficients, intercepts and statistical parameters are presented in Table 8. At times, when the fuel was being changed over from LNG to MGO and vice versa, fuel consumption values produced negative predicted NO_x emission rate values. When these were omitted, the correlation between predicted and observed values for all three engines was 0.88 (95% CI 0.88–0.88, p<0.01), the adjusted r^2 0.77 and the RMSE 1.15 (Fig. 11).

As the NO_x emissions of dual-fuel engines in gas mode can be assumed to be compliant with Tier 3 limits, there is no need to model them differently whether the vessel is in or outside NECA.

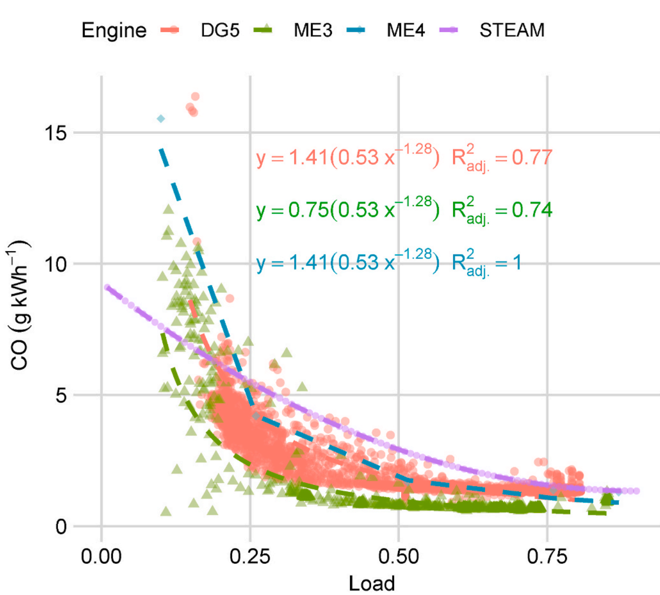

Fig. 9. Emission factor for CO (g kWh^{-1}) for ME3, ME4, DG5 and STEAM with corresponding colours and shapes. Fitted exponential regression with dashed lines. (For interpretation of the references to colour in this figure legend, the reader is referred to the Web version of this article.)

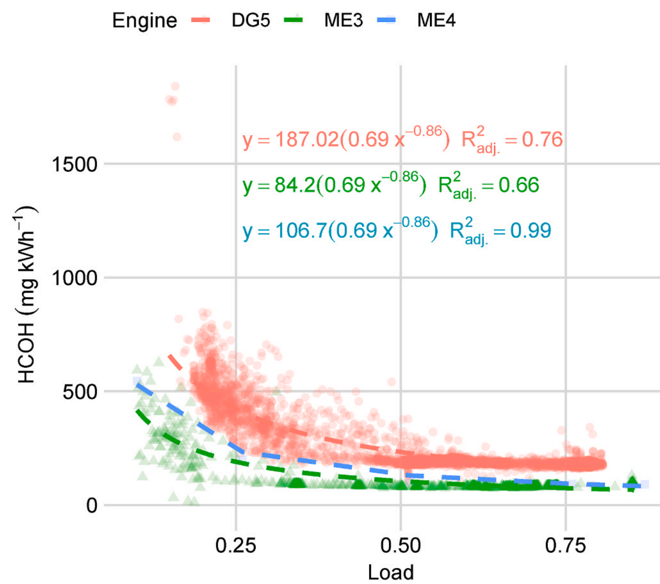

Fig. 10. Emission factor for HCOH (mg kWh^{-1}) for ME3, ME4 and DG5 with corresponding colours and shapes. Fitted exponential regressions with dashed lines. (For interpretation of the references to colour in this figure legend, the reader is referred to the Web version of this article.)

3.7. Comparison between fuel-based emission factor calculation methods

The fuel-based emission factor of an exhaust gas component can be estimated to a reasonable degree of accuracy with the default LNG carbon content of 0.75 using the molar mass method described with formulas 9, 10 and 11 from a dual-fuel engine as long as the share of pilot fuel is taken in account. The calculated emission factors for CH_4, CO and HCOH were in good agreement with ones calculated with precise fuel composition and consumption data using the IMO NO_x Technical Code carbon balance method: the Pearson's correlation between the emission factors for CH_4 measured from ME3 was 0.97 (95% CI 0.96–0.97, p<0.01), for CO 1.00 (95% CI 1.00–1.00, p<0.01) and for HCOH 0.99 (95% CI 0.99–0.99, p<0.01). The correlation between all three exhaust gas compounds measured from DG5 was 1.00 (95% CI 1.00–1.00, p<0.01). However, the share of pilot fuel causes significant uncertainty in the calculation: while the molar mass method over-predicts the CH_4 and CO measured from DG5 by 1%–2%, it under-predicts the same compounds measured from ME3 by 49%–59% (Table 9 and Fig. 12).

3.8. Operational mode analysis

Both measurement campaigns revealed that exhaust gas components can be modelled to a reasonable degree of accuracy when the ship is in normal operation, but significantly higher concentrations of all components were observed at times generating outliers in the data. When the

Table 8
Coefficients α and β and the intercept γ and adjusted r^2 for the NO_x emission rate for the three measured engines. The coefficients and intercept were statistically significant (p<0.05) only for the engine DG5.

Eng.	α	95%CI		β	95%CI		γ	95%CI		r^2
DG5	0.07	0.07	0.07	4.92	4.80	5.03	−54.70	−56.10	−53.30	0.39
ME3	0.00	−0.02	0.01	0.12	−0.19	0.43	−1.28	−4.64	2.08	0.70
ME4	0.01	−0.05	0.08	8.71	−34.77	52.19	−39.66	−246.89	167.58	0.27

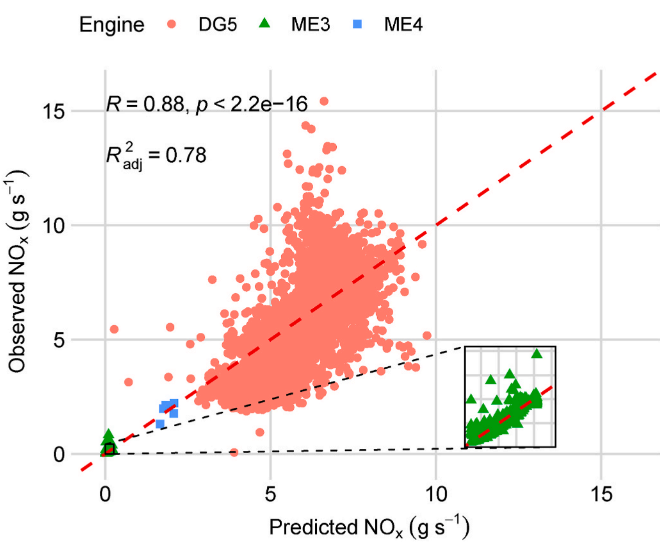

Fig. 11. Predicted NO_x emission rate (in g s^{-1}) using formula 23 together with the coefficients of Table 8 on x-axis and the observed NO_x emission rate on y-axis of the three measured engines with a zoom in to the values for ME3. The red dashed line represents 1:1 correlation. (For interpretation of the references to colour in this figure legend, the reader is referred to the Web version of this article.)

Table 9
Coefficient α and intercept β with 95% confidence intervals and adjusted r^2 for linear regression between EF_{IMO} and EF_{mm} for CH_4, CO and HCOH measured from engines ME3 (top of table) and DG5 (bottom of table).

ME3	α	CI		β	CI		R^2
CH_4	1.59	1.56	1.61	−0.003	−0.003	−0.003	0.93
CO	1.49	1.48	1.49	−0.001	−0.002	−0.001	1.00
HCOH	1.58	1.57	1.59	−0.163	−0.169	−0.158	0.99
DG5	α	CI		β	CI		R^2
CH_4	0.99	0.99	1.00	0.001	0.001	0.001	0.99
CO	0.99	0.99	0.99	0.001	0.001	0.001	0.99
HCOH	0.98	0.98	0.99	0.094	0.092	0.096	0.99

mean raw emission rates (in g s^{-1} or mg s^{-1}) were analysed between different operational modes, for both campaigns the highest CO_2, CH_4 and HCOH emissions occurred while the ship was at sea, the second highest at the manoeuvring phase and lowest when the ship was alongside in port (Table 10). This is logical as an increase in speed increases fuel consumption and therefore leads to increased emissions rates. However, the CO emission rate was highest during the manoeuvring phase and lowest at sea in campaign 1. Also, NO_x emission rates were highest in ports in both campaigns when the engine was running. As the operational modes were based on speed, port phases include times when the ship is preparing for departure and immediately after arrival, when the speed is zero, but non-optimal engine configurations are used and engines are started and stopped.

4. Discussion

The two measuring campaigns revealed that the CH_4 slip from a 4-stroke low-pressure dual-fuel engine operated in a diesel-electric setup is dependent on both engine load and the share of pilot fuel of total energy consumption. However, the shape of the curve of the CH_4 slip using only engine load as the dependent variable seems parabolic on the first campaign engines and exponential on the second campaign engine. This could be because the campaign 2 engine was not run >80% load and therefore there is no data on higher loads. CH_4 slip modelling seems to be more accurate using the fuel consumption rates for the LNG gas and pilot fuel. This knowledge can be used to model methane emissions from similar ships with more precision as current efforts to quantify total CH_4 emissions from LNG-powered vessels use weighted average emission factors (Pavlenko et al., 2020; Faber et al., 2020) omitting the variations in engine load and share of pilot fuel consumption. Bottom-up modelling can be used to have a better understanding of used engine loads to calculate appropriate weighting factors for the test cycles defined in the IMO NO_x Techical Code.

The development engine (ME3) measured during campaign 1 produced a reduced CH_4 slip compared to the standard engine ME4 and the engine measured during campaign 2. However, this is mostly achieved with a significant increase in the share of pilot fuel in the total energy consumption. As the carbon content of the pilot fuel is larger than with LNG gas, this leads to increased CO_2 and particle emissions and therefore partly losing the benefits of using LNG as fuel. Lehtoranta et al. (2023) calculated that the greenhouse gas output in carbon dioxide equivalents (CH_4 + CO_2) of ME3 is still less than with ME4 with all the measured engine load points. Lehtoranta et al. (2023) used the 100-year global warming potential (GWP100) of 29.8 for CH_4. Balcombe et al. (2022) measured CH_4 slip on board a LNG carrier and used the GWP100 of 36 for CH_4 based on Balcombe et al. (2021). The average CH_4 slip across all engines was 3.8% of which most was caused by the low-pressure dual-fuel auxiliary engines, which had a mean CH_4 slip of 8.2%. More measurements should be made also on board vessels that use conventional propulsion, where the engine revolutions can be varied with the engine load and include black carbon (BC) measurements as increasing pilot fuel consumption might lead to an increased BC, which also contributes to global warming.

The CH_4 slip's load-dependency influences the vessel's total methane emissions. From 2026 ships will need allowances not only for their CO_2 emissions but also for CH_4 and nitrous oxide (N_2O) emissions when travelling within, to, or from European Union ports. Also, in the FueEU Maritime regulation ships are fined if they exceed the annual greenhouse gas intensity index (g CO_2e MJ^{-1}), where CH_4 slip is also accounted for. The intensity index is calculated on Well-to-Wake basis, and the upstream emissions of LNG (18.5 g CO_2e MJ^{-1}) are higher than with oil-based fuels (HFO: 13.5 g CO_2e MJ^{-1}, LFO: 13.2 g CO_2e MJ^{-1} and MGO/MDO:14.4 g CO_2e MJ^{-1}). The CH_4 slip from 4-stroke low-pressure dual-fuel engines is currently defined as 3.1% of gas consumed in the regulation including both slipped and fugitive emissions. It is questionable if a constant methane slip is fair or unfair for those who need to pay for the allowances. The regulation stipulates that CH_4 slip is measured at 50% engine load, and our results indicate that from the three measured engines, the slip at this load was less than 3.1% (0.9%–2.4%). If the engine load can be kept high, the total methane emissions from these engines are probably less than 3.1%, but if the load

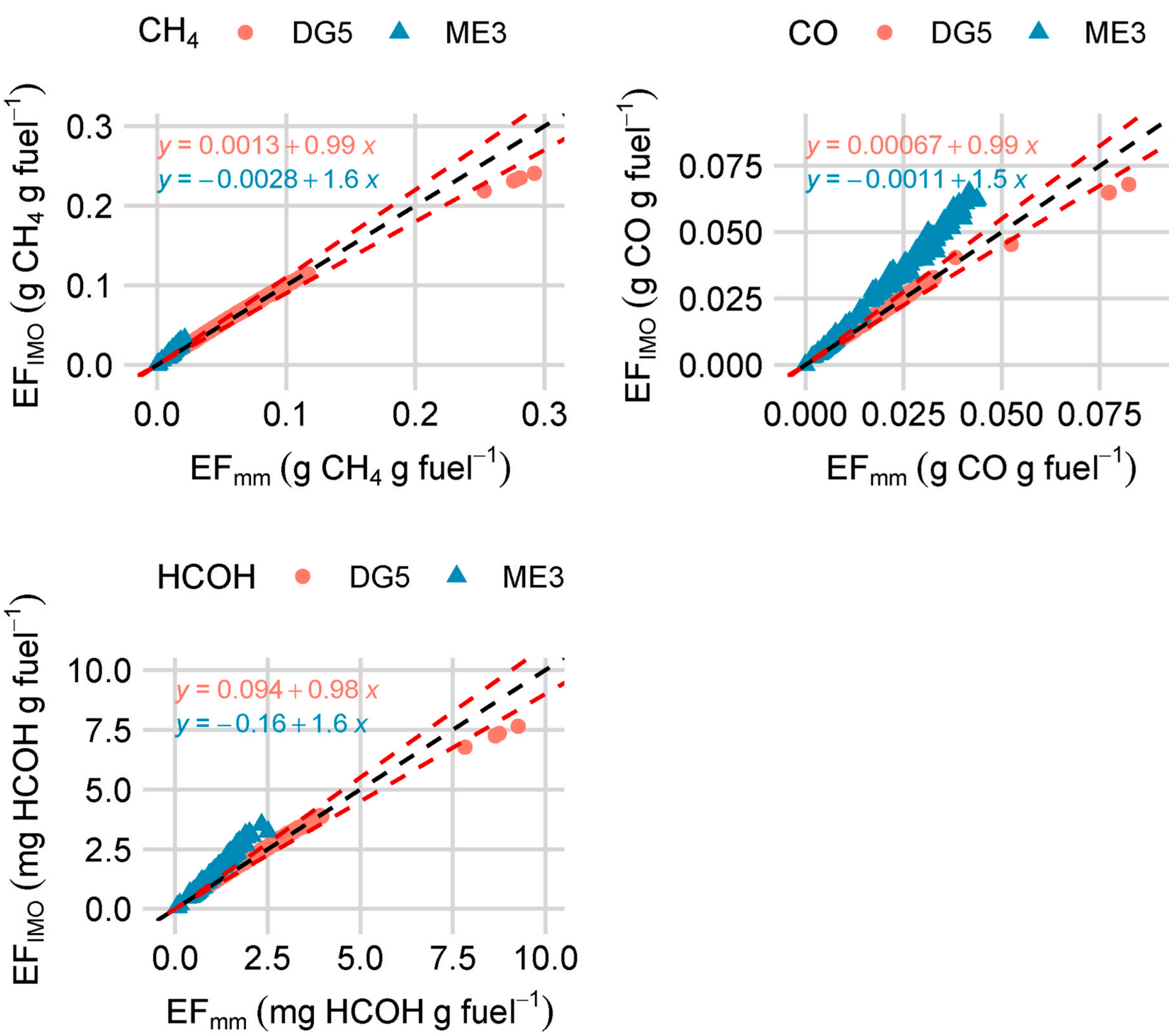

Fig. 12. Fuel-based emission factors (*g g fuel*$^{-1}$ for CH_4 and CO and *mg g fuel*$^{-1}$ for HCOH) measured from engines DG5 (red circles) and ME3 (green triangles) for CH_4 (top left), CO (top right) and HCOH (bottom) calculated with the molar mass method (E_{mm}) on x-axis and with the IMO NO_x Technical Code mass balance method (EF_{IMO}) The black dashed line represents 1:1 agreement and the red dashed lines 10% under and over predictions. (For interpretation of the references to colour in this figure legend, the reader is referred to the Web version of this article.)

Table 10
Mean emission rates (g s^{-1}, * mg s^{-1} for HCOH) of exhaust gas components while the vessel was at berth (B), manoeuvring (M) and at sea (S) and of campaigns 1 and 2.

Pollutant	B1	M1	S1	B2	M2	S2
CO_2	139.3	179.7	378.8	1155.1	1450.0	1487.5
CH_4	0.5	0.6	1.2	8.0	8.8	8.9
CO	0.8	1.2	0.7	3.7	4.3	4.5
HCOH*	47.8	54.2	67.0	471.8	558.5	585.3
NO_x	0.3	0.1	0.2	6.7	6.0	5.5

is variable or constantly kept low, true emissions might be higher than 3.1% of gas consumed. Port emissions play a significant role in the total CH_4 slip: the auxiliary power demand might not be high enough to keep adequate engine load for decreased CH_4 slip and ship crew don't want to risk having blackouts in port if sudden peaks of auxiliary power demand occur. This will be partially solved in EU ports with the FuelEU Maritime regulation that requires passenger and container vessels to connect to shore power or other emission-free power sources if the port call is longer than 2 h by 2030. This requirement also addresses some of the issues of air quality, which is affected by the increased CO and HCOH emissions produced by LNG-powered vessels. Peng et al. (2020) calculated that these air pollutants might cause health risks that outweigh the reductions of NO_x and PM emissions caused by fuel oil-powered ships. However, as observed in this study, high emissions in ports occur when the main engines are started and stopped.

Another point to be considered is that methane concentration was measured directly from the exhaust in both measuring campaigns. Methane could escape the engine via the piston rings to the crankcase and exit into the atmosphere via the engine room ventilation as shown by Delprete et al. (2019). An estimate of 1 g kWh^{-1} for this was suggested by Ushakov et al. (2019). Also, in a setup where the ship has conventional propulsion, a large part of the methane slip will be generated from the auxiliary engines as pointed out by Balcombe et al. (2022). In addition, there could be fugitive methane emissions from the vessel anywhere along the fuel tank and the engine, specifically during bunkering as shown by Comer et al. (2024). Evidence gathered from studies, where methane was measured outside the vessel hints that the true absolute methane emissions are larger than only those measured from the exhaust of the main engine. In Grönholm et al. (2021) methane was measured at a remote marine station from passing vessel exhaust gas plumes. Ships equipped with low-pressure 4-stroke main engines had exhaust gas plumes with CH_4 to CO_2 ratios between 1.2% and 9.3% with a median of around 3%. As the fuel factor of CH_4 for LNG is 1.00 (Table 2), this ratio represents the CH_4 slip to a reasonable degree of accuracy depending on the share of pilot fuel used, and with increased pilot fuel share, the concentration ratio of CH_4/CO_2 is an underestimate. In Comer et al. (2024) CH_4 slip measured using drones from LNG-powered ships equipped with low-pressure 4-stroke engines had a median of 6.1%.

The fuel carbon content (FCC) varied between the vessels: the LNG used in campaign 1 had FCC 75.3% whereas in campaign 2 it was 75.1%. The pilot fuel in campaign 1 had FCC 84.4% and in campaign 2 86.7%. These also differ from the IMO default values (75.0% for LNG and 87.0% for MGO). The FCC defines the emission factor for CO_2: the LNG used in campaign 1 has EF_{CO_2} of 2.76 and the LNG in campaign 2 2.75. The pilot fuel in campaign 1 has EF_{CO_2} of 3.09 and the pilot fuel in campaign 2 3.18. The default EF_{CO_2} for LNG is 2.75 and for MGO/MDO 3.21 in IMO regulation and in the FuelEU Maritime directive (International Maritime Organisation, 2008; Regulation (EU) 2023/1805, 2023).

Fuel-based emission factors calculated from the ratio of concentrations between exhaust gas compounds and CO_2 using the molar mass method correlated almost perfectly with ones calculated using the IMO NO_x Technical Code carbon balance method together with precise fuel composition and consumption data. However, the increased share of pilot fuel of ME3 leads to around 50% underprediction. It is also worth noting, that the generic hydrocarbon density ratio should not be used for converting CH_4 and HCOH. Instead, the density ratios need to be calculated or taken from the ISO Standard 8178-1 (ISO, 2006) for these compounds as they are not provided in Table 5 of the NO_x Technical code bearing in mind also that the exhaust gas density for natural gas seems to be wrong in Table 5 (1.2611 when should be 1.2661).

Surprisingly NO_x emissions seem to decrease even with an increase in pilot fuel share of total energy consumption measured from the development engine ME3. The effort to minimise CH_4 slip with an increase of pilot fuel share seems to solve two issues: the CH_4 slip and NO_x emissions with the drawback of increased particle number and CO_2 (Lehtoranta et al., 2023) and probably SO_2.

LNG gas was used on both engines onboard the first studied vessel even with engine loads <20% based on measured CH_4 concentration, which was not the case onboard the passenger ferry vessel used in the works of Anderson et al. (2015), where only MGO was consumed with engine load of 16% when the vessel was alongside. The ratio between pilot fuel and gas should therefore be reconsidered in the modelling of dual-fuel vessels and their emissions.

Emission factors are often represented as factors or formulas with mean values or point estimates without confidence or prediction intervals. This does not give an accurate representation of true emissions as can be seen from the emission factors calculated from raw measuring data. A more precise presentation would be to express the error margin with the lower and upper bound.

More measured data is needed to make definitive conclusions which can be used to finetune modelling parameters for different LNG-powered ships, especially concerning pollutants that affect air quality and when engines are turned on and off.

5. Conclusions

The resistance calculation method used in the STEAM model delivers reasonably accurate results. However, the additional resistance created by meteorological factors probably needs to be updated. Also, the current methodology to predict auxiliary power demand underestimates the true auxiliary power demand on large cruise ships. More research is needed to have a better understanding of modelling auxiliary power demand on ships.

Connecting ships to shore power or similar systems eliminates the combustion-based emissions from auxiliary power demand during the port calls. This is only possible if a shore power connection exists in both the port and on board the vessel. This needs to be included in the modelling.

Internal combustion engines used in constant-speed setups need to be modelled with specific fuel consumption curves to accurately predict consumption specifically on low engine loads. Pilot fuel consumption needs to be taken into account as it has a significant effect on emission factors.

Methane slip from LNG-powered low-pressure 4-stroke dual-fuel engines varies as a function of engine load and with the share of pilot fuel of the total energy consumption. LNG-powered dual-fuel engines produce carbon monoxide and formaldehyde emissions that are dependent on engine load. Short bursts of high emissions of NO_x can be observed when engines are started.

The ratio between measured exhaust gas compound and carbon dioxide can be used to calculate fuel-based emission factors. This can be used for research and emission monitoring.

CRediT authorship contribution statement

Mikko Heikkilä: Writing – review & editing, Writing – original draft, Visualization, Validation, Software, Project administration, Methodology, Investigation, Formal analysis, Conceptualization. **Niina Kuittinen:** Writing – review & editing, Data curation. **Tiia Grönholm:** Writing – review & editing, Validation, Supervision, Software, Resources, Methodology, Data curation.

Declaration of competing interest

The authors declare that they have no known competing financial interests or personal relationships that could have appeared to influence the work reported in this paper.

Data availability

The data that has been used is confidential.

Acknowledgements

This research is a part of the European Union project GREEN RAY which has received funding from the European Union's Horizon 2020 – Research and Innovation Framework Programme action under grant agreement No 101056642.

References

Aakko-Saksa, P.T., Lehtoranta, K., Kuittinen, N., Järvinen, A., Jalkanen, J.P., Johnson, K., Jung, H., Ntziachristos, L., Gagné, S., Takahashi, C., Karjalainen, P., Rönkkö, T., Timonen, H., 2023. Reduction in greenhouse gas and other emissions from ship engines: current trends and future options. Prog. Energy Combust. Sci. 94, 101055 https://doi.org/10.1016/j.pecs.2022.101055.

Alanen, J., Isotalo, M., Kuittinen, N., Simonen, P., Martikainen, S., Kuuluvainen, H., Honkanen, M., Lehtoranta, K., Nyyssönen, S., Vesala, H., Timonen, H., Aurela, M., Keskinen, J., Rönkkö, T., 2020. Physical characteristics of particle emissions from a medium speed ship engine fueled with natural gas and low-sulfur liquid fuels. Environ. Sci. Technol. 54, 5376–5384. https://doi.org/10.1021/acs.est.9b06460.

Altarriba, E., Rahiala, S., Tanhuanpää, T., 2024. Comparative study of lng/mgo emission levels on a ropax ship. J. Marit. Res. 21, 140–152.

Anderson, M., Salo, K., Fridell, E., 2015. Particle- and gaseous emissions from an LNG powered ship. Environ. Sci. Technol. 49, 12568–12575. https://doi.org/10.1021/acs.est.5b02678.

Balcombe, P., Heggo, D.A., Harrison, M., 2022. Total methane and CO_2 emissions from liquefied natural gas carrier ships: the first primary measurements. Environ. Sci. Technol. 56, 9632–9640. https://doi.org/10.1021/acs.est.2c01383.

Balcombe, P., Staffell, I., Kerdan, I.G., Speirs, J.F., Brandon, N.P., Hawkes, A.D., 2021. How can LNG-fuelled ships meet decarbonisation targets? An environmental and economic analysis. Energy 227, 120462. https://doi.org/10.1016/j.energy.2021.120462.

Blendermann, W., 1994. Parameter identification of wind loads on ships. J. Wind Eng. Ind. Aerod. 51, 339–351. https://doi.org/10.1016/0167-6105(94)90067-1.

Box, G., Draper, N., 1987. Empirical Model-Building and Response Surfaces. John Wiley and Sons.

Box, G.E.P., 1976. Science and statistics. J. Am. Stat. Assoc. 71, 791–799. https://doi.org/10.1080/01621459.1976.10480949.

Burel, F., Taccani, R., Zuliani, N., 2013. Improving sustainability of maritime transport through utilization of liquefied natural gas (LNG) for propulsion. Energy 57, 412–420. https://doi.org/10.1016/j.energy.2013.05.002.

Chen, X., Yang, J., 2024. Analysis of the uncertainty of the ais-based bottom-up approach for estimating ship emissions. Mar. Pollut. Bull. 199, 115968 https://doi.org/10.1016/j.marpolbul.2023.115968. https://www.sciencedirect.com/science/article/pii/S0025326X23014030.

Comer, B., Beecken, J., Vermeulen, R., Sturrup, E., Paschinger, P., Osipova, L., Gore, K., Delahaye, A., Verhagen, V., Knudsen, B., Knudsen, J., Verbeek, R., 2024. Fugitive and unburned methane emissions from ships (FUMES). In: Technical Report. ICCT. https://theicct.org/wp-content/uploads/2023/11/ID-64-%E2%80%93-FUMES-ships-Report-A4-60037-FV.pdf.

Delprete, C., Selmani, E., Bisha, A., 2019. Gas escape to crankcase: impact of system parameters on sealing behavior of a piston cylinder ring pack. Int J Energy Environ Eng 10, 207–220. https://doi.org/10.1007/s40095-019-0296-x.

Ekanem Attah, E., Bucknall, R., 2015. An analysis of the energy efficiency of lng ships powering options using the eedi. Ocean Eng. 110, 62–74. https://doi.org/10.1016/j.oceaneng.2015.09.040.energyEfficientShipDesignandOperations.

Faber, J., Hanayama, S., Zhang, S., Pereda, P., Comer, B., Hauerhof, E., van der Loeff, W. S., Smith, T., Zhang, Y., Kosaka, H., Adachi, M., Bonello, J.M., Galbraith, C., Gong, Z., Hirata, K., Hummels, D., Kleijn, A., Lee, D.S., Liu, Y., Lucchesi, A., Mao, X., Muraoka, E., Osipova, L., Qian, H., Rutherford, D., de la Fuente, S.S., Yuan, H., Perico, C.V., Wu, L., Sun, D., Yoo, D.H., Xing, H., 2020. Fourth IMO GHG study. https://www.imo.org/en/OurWork/Environment/Pages/Fourth-IMO-Greenhouse-Gas-Study-2020.aspx.

Golub, G., Pereyra, V., 2003. Separable nonlinear least squares: the variable projection method and its applications. Inverse Probl. 19 https://doi.org/10.1088/0266-5611/19/2/201.

Grigoriadis, A., Mamarikas, S., Ioannidis, I., Majamäki, E., Jalkanen, J.P., Ntziachristos, L., 2021. Development of exhaust emission factors for vessels: a review and meta-analysis of available data. Atmos. Environ. X 12, 100142. https://doi.org/10.1016/j.aeaoa.2021.100142.

Grönholm, T., Mäkelä, T., Hatakka, J., Jalkanen, J.P., Kuula, J., Laurila, T., Laakso, L., Kukkonen, J., 2021. Evaluation of methane emissions originating from LNG ships based on the measurements at a remote marine station. Environ. Sci. Technol. 55, 13677–13686. https://doi.org/10.1021/acs.est.1c03293.

Guo, B., Liang, Q., Tvete, H.A., Brinks, H., Vanem, E., 2022. Combined machine learning and physics-based models for estimating fuel consumption of cargo ships. Ocean Eng. 255, 111435 https://doi.org/10.1016/j.oceaneng.2022.111435.

Hollenbach, Klaus U., 1999. Estimating resistance and propulsion for single-screw and twin-screw ships in the preliminary design. In: Proceedings of the International Conference on Computer Applications in Shipbuilding, pp. 237–250.

International Maritime Organisation, 2008. NOx Technical Code – Resolution MEPC.177 (58), Amendments to the Technical Code on Control of Emission of Nitrogen Oxides from Marine Diesel Engines.

IPCC, 2014. Anthropogenic and natural radiative forcing. In: Technical Report. IPCC. https://doi.org/10.1017/CBO9781107415324.018.

ISO, 2006. International Standard Iso 8178-1. Reciprocating Internal Combustion Engines - Exhaust Gas Emission Measurement.

Jalkanen, J.P., Brink, A., Kalli, J., Pettersson, H., Kukkonen, J., Stipa, T., 2009. A modelling system for the exhaust emissions of marine traffic and its application in the baltic sea area. Atmos. Chem. Phys. 9, 9209–9223. https://doi.org/10.5194/acp-9-9209-2009.

Jalkanen, J.P., Johansson, L., Kukkonen, J., Brink, A., Kalli, J., Stipa, T., 2012. Extension of an assessment model of ship traffic exhaust emissions for particulate matter and carbon monoxide. Atmos. Chem. Phys. 12, 2641–2659. https://doi.org/10.5194/acp-12-2641-2012.

Jensen, T.K., Schramm, J., Morgen, C., 1999. Unburned hydrocarbon emissions from si engines using gaseous fuels. SAE Trans. 108, 915–926. URL: http://www.jstor.org/stable/44743424.

Johansson, L., Jalkanen, J.P., Kukkonen, J., 2017. Global assessment of shipping emissions in 2015 on a high spatial and temporal resolution. Atmos. Environ. 167, 403–415. https://doi.org/10.1016/j.atmosenv.2017.08.042.

Juva, M., Riska, K., 2002. Research report 53: on the power requirements in the Finnish-Swedish ice class rules. In: Technical Report. Helsinki University of Technology.

Kim, Y.R., Steen, S., Kramel, D., Muri, H., Strømman, A.H., 2023. Modelling of ship resistance and power consumption for the global fleet: the MariTEAM model. Ocean Eng. 281, 114758 https://doi.org/10.1016/j.oceaneng.2023.114758.

Kuittinen, N., Heikkilä, M., Lehtoranta, K., 2023. Review of methane slip from LNG engines. In: Technical Report. Green Ray Project. https://greenray-project.eu/wp-content/uploads/2023/04/D1.1_Review_of_methane_slip_from_LNG_engines.pdf.

Lehtoranta, K., Kuittinen, N., Vesala, H., Koponen, P., 2023. Methane emissions from a State-of-the-Art LNG-powered vessel. Atmosphere 14. https://doi.org/10.3390/atmos14050825.

Moreno-Gutiérrez, J., Calderay, F., Saborido, N., Boile, M., Rodríguez Valero, R., Durán-Grados, V., 2015. Methodologies for estimating shipping emissions and energy consumption: a comparative analysis of current methods. Energy 86, 603–616. https://doi.org/10.1016/j.energy.2015.04.083.

Moreno-Gutiérrez, J., Durán-Grados, V., 2021. Calculating ships' real emissions of pollutants and greenhouse gases: towards zero uncertainties. Sci. Total Environ. 750, 141471 https://doi.org/10.1016/j.scitotenv.2020.141471.

Nielsen, Joergen, B., Stenersen, D., 2010. Emission factors for CH_4, NO_x, particulates and black carbon for domestic shipping in Norway, revision 1. In: Technical Report. MARINTEK. https://www.osti.gov/etdeweb/biblio/1005100.

Nunes, R., Alvim-Ferraz, M., Martins, F., Sousa, S., 2017. The activity-based methodology to assess ship emissions - a review. Environ. Pollut. 231, 87–103. https://doi.org/10.1016/j.envpol.2017.07.099.

Pavlenko, N., Comer, B., Zhou, Y., Clark, N.N., Rutherford, D., 2020. The climate implications of using LNG as a marine fuel. In: Technical Report. ICCT. https://theicct.org/wp-content/uploads/2021/06/LNG-as-marine-fuel-working-paper-02_FINAL_20200416.pdf.

Peng, W., Yang, J., Corbin, J., Trivanovic, U., Lobo, P., Kirchen, P., Rogak, S., Gagné, S., Miller, J.W., Cocker, D., 2020. Comprehensive analysis of the air quality impacts of switching a marine vessel from diesel fuel to natural gas. Environ. Pollut. 266, 115404 https://doi.org/10.1016/j.envpol.2020.115404.

Regulation (EU) 2023/1805, 2023. Regulation (EU) 2023/1805 of the European Parliament and of the Council of 13 September 2023 on the Use of Renewable and Low-Carbon Fuels in Maritime Transport, and Amending Directive 2009/16/EC (Text with EEA Relevance).

Riska, K., Wilhelmson, M., Englund, K., Leiviskä, T., 1997. Research report 52: performance of merchant vessels in ice in the Baltic. In: Technical Report. Helsinki University of Technology.

Rochussen, J., Jaeger, N., Penner, H., Khan, A., Kirchen, P., 2023. Development and demonstration of strategies for ghg and methane slip reduction from dual-fuel natural gas coastal vessels. Fuel 349, 128433. https://doi.org/10.1016/j.fuel.2023.128433.

Sharafian, A., Blomerus, P., Mérida, W., 2019. Natural gas as a ship fuel: assessment of greenhouse gas and air pollutant reduction potential. Energy Pol. 131, 332–346. https://doi.org/10.1016/j.enpol.2019.05.015.

Sommer, D.E., Yeremi, M., Son, J., Corbin, J.C., Gagné, S., Lobo, P., Miller, J.W., Kirchen, P., 2019. Characterization and reduction of in-use ch4 emissions from a dual fuel marine engine using wavelength modulation spectroscopy. Environ. Sci. Technol. 53, 2892–2899.

Stenersen, D., Thonstad, O., 2017. GHG and NOx emissions from gas fuelled engines. In: Technical Report. SINTEF. https://www.nho.no/siteassets/nox-fondet/rapporter/2018/methane-slip-from-gas-engines-mainreport-1492296.pdf.

Thomson, H., Corbett, J.J., Winebrake, J.J., 2015. Natural gas as a marine fuel. Energy Pol. 87, 153–167. https://doi.org/10.1016/j.enpol.2015.08.027.

Townsin, R.L., Kwon, Y.J., 1983. Approximate formulae for the speed loss due to added resistance in wind and waves. RINA Supplem. Papers 125, 99.

Townsin, R.L., Kwon, Y.J., 1993. Estimating the influence of weather on ship performance. RINA Transactions 135, 191.

Ushakov, S., Stenersen, D., Einang, P.M., 2019. Methane slip from gas fuelled ships: a comprehensive summary based on measurement data. Marine Sci. Tech. https://doi.org/10.1007/s00773-018-00622-z.